Forschungszentrum Karlsruhe
in der Helmholtz-Gemeinschaft

Wissenschaftliche Berichte
FZKA 6937

T-stress Solutions Determined by Finite Element Computations

T. Fett, G. Rizzi

Institut für Materialforschung

August 2004

FORSCHUNGSZENTRUM KARLSRUHE

in der Helmholtz-Gemeinschaft

Wissenschaftliche Berichte

FZKA 6937

T-STRESS SOLUTIONS DETERMINED BY FINITE ELEMENT COMPUTATIONS

T. Fett, G. Rizzi

Institut für Materialforschung

Forschungszentrum Karlsruhe GmbH, Karlsruhe

2004

Impressum der Print-Ausgabe:

Als Manuskript gedruckt

Forschungszentrum Karlsruhe GmbH
Postfach 3640, 76021 Karlsruhe

Mitglied der Hermann von Helmholtz-Gemeinschaft
Deutscher Forschungszentren (HGF)

ISSN 0947-8620

urn:nbn:de:0005-069370

T-stress solutions determined by finite element computations

Abstract:

Failure of cracked components is caused by the stresses in the vicinity of the crack tip. The singular stress contribution is characterised by the stress intensity factor K, the first regular stress term is represented by the so-called T-stress.

While stress intensity factor solutions are reported in handbooks for many crack types and loading cases, T-stress terms are available only for a small number of test specimens and simple loading cases, such as for instance pure tension and bending.

T-stress solutions for components containing edge cracks were computed by application of the Finite Element Method (FEM). The results are compiled in form of figures, tables or approximate relations. Since the stress intensity factors also arise during T-computations, they are reported, too.

In addition, Green's functions for T-stresses are quoted, which enable to compute T-stress terms for any given stress distribution in the uncracked body.

T-Spannungslösungen aus Finite-Elemente Berechnungen

Kurzfassung:

Das Versagen von Bauteilen mit Rissen wird durch die unmittelbar an der Rissspitze auftretenden Spannungen verursacht. Der singuläre Anteil diese Spannungen wird durch den Spannungsintensitätsfaktor K charakterisiert. Der erste reguläre Term wird durch die so genannte T-Spannung beschrieben.

Während K-Lösungen für viele Probengeometrien in Handbüchern enthalten sind, sind Lösungen für die T-Spannung nur für einfache Geometrien verfügbar.

Im vorliegenden Bericht werden Ergebnisse mitgeteilt, die mit der "Finite-Elemente Methode" (FEM) bestimmt wurden. Die Resultate werden in Form von Diagrammen, Tabellen und Näherungsformeln wiedergegeben. Da im Zuge der T-Berechnungen auch die Spannungsintensitätsfaktoren anfallen, wurden auch diese aufgenommen.

Zusätzlich werden Greensfunktionen für T angegeben. Diese erlauben die Berechnung des T-Spannungsterms für beliebige Spannungsverteilungen in der ungerissenen Struktur.

Contents

1. Introduction

In the case of symmetric crack problems, the stress components in the surroundings of a crack tip are given by

$$\frac{\sigma_r}{\sigma^*} = \sum_{n=0}^{\infty} A_n (r/W)^{n-1/2} (n+3/2) \left[\frac{n^2 - 2n - 5/4}{n - 1/2} \cos(n-1/2)\varphi - (n+1/2)\cos(n+3/2)\varphi \right]$$

$$+ \sum_{n=0}^{\infty} A^*_n (r/W)^n [(n^2 - n - 2)\cos n\varphi - (n+2)(n+1)\cos(n+2)\varphi] \tag{1.1}$$

where r and φ are polar coordinates with the origin at the crack tip (Fig. 1.1). Taking into consideration the singular stress term and the first regular term, the near-tip stress field for a mode-I crack can be described by

$$\sigma_{ij} = \frac{K_I}{\sqrt{2\pi r}} f_{ij}(\varphi) + \sigma_{ij,0} \tag{1.2}$$

In Cartesian coordinates, the regular stress term reads

$$\sigma_{ij,0} = \begin{pmatrix} \sigma_{xx,0} & \sigma_{xy,0} \\ \sigma_{yx,0} & \sigma_{yy,0} \end{pmatrix} = \begin{pmatrix} T & 0 \\ 0 & 0 \end{pmatrix} \tag{1.3}$$

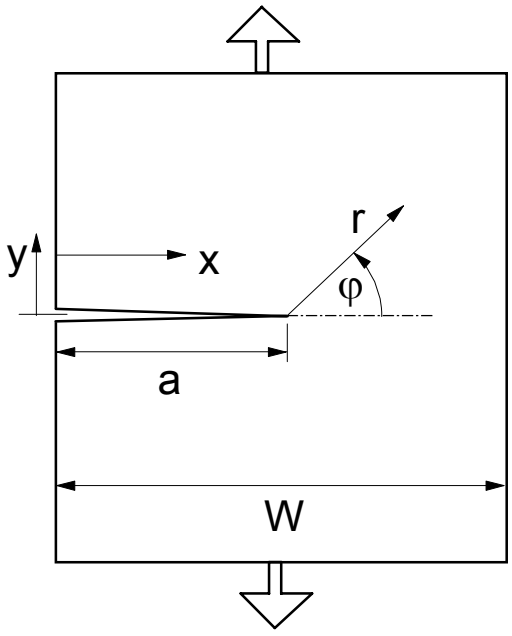

Fig. 1.1 Geometrical data of a crack in a finite component.

The term with the coefficient A^*_0 in eq.(1.1) represents the total constant σ_x-stress contribution at the crack tip ($x = a$) of a cracked structure, which is called the T-stress

$$T = \sigma_x(\varphi = \pi)\big|_{x=a} = -4\sigma^* A^*_0 \ . \tag{1.4}$$

If the normal stress component on the crack faces does not disappear (this is the case for e.g. a pressurized crack), T is given as

$$T = \sigma_x\big|_{x=a} - \sigma_y\big|_{x=a} \tag{1.5}$$

2. Representation of T-stresses by a Green's function

As a consequence of the principle of superposition, stress fields for different loadings can be added in the case of single loadings acting simultaneously. This leads to an integration of the loading parameters. It was applied very early to the singular stress field and the computation of the related stress intensity factor by Bückner [1]. Similarly, the T-stress contribution T_c caused by the crack exclusively can be expressed by an integral [2-8]. The integral representation reads

$$T = \int_0^a t(x,a)\sigma_y(x)dx \tag{2.1}$$

where the integration has to be performed using the stress field σ_y in the uncracked body. The stress contributions are weighted by a weight function (h, t) depending on the location x, where the stress σ_y acts.

2.1 Asymptotic term

In order to describe the Green's function, it is distinguished between a term t_0 representing the asymptotic limit case of near-tip behaviour and an additive regular term t_{reg} which includes information about the special shape of the component and the finite dimensions,

$$t = t_0 + t_{reg} \tag{2.2}$$

In order to obtain information on the asymptotic behaviour of the weight or Green's function, near-tip behaviour is considered exclusively. Therefore a small section of the body (dashed circle) very close to the crack tip (Fig. 2.1) is taken. The near-tip zone is zoomed very strongly. Consequently, the outer borders of the component move to infinity. Now, the case of a semi-infinite crack in an infinite body is obtained. If the crack faces are loaded by a couple of forces P at location $x=x_0$ with $a-x_0 \ll a$, the stress state can be described by the Westergaard stress function [9]:

$$Z = \frac{P}{\pi}\frac{1}{z+b}\sqrt{\frac{b}{z}}\,, \quad z = \xi + iy\,, \quad \xi = x - a \tag{2.3}$$

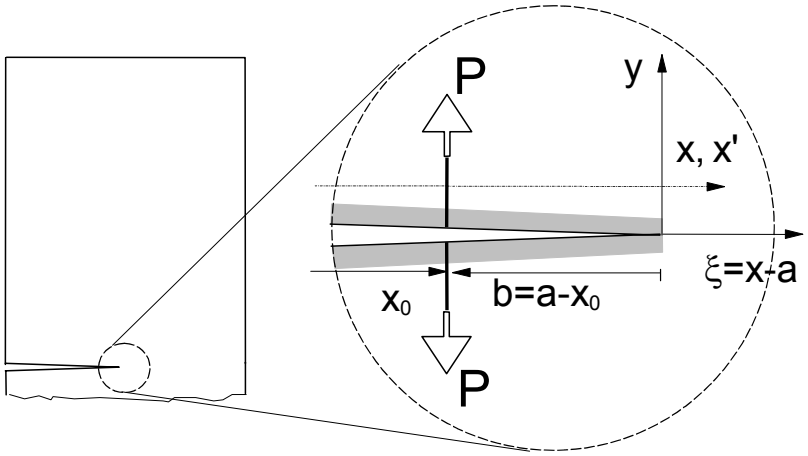

Fig. 2.1 Situation at the crack tip for asymptotic stress consideration.

The regular contribution to the stress function is (z, $b \neq 0$)

$$Z_{reg} = -\frac{P}{\pi}\frac{1}{z+b}\sqrt{\frac{z}{b}} \tag{2.4}$$

from which the regular part of the x-stress component results as

$$\sigma_x = \mathrm{Re}\, Z - y\,\mathrm{Im}(dZ/dz) \;\Rightarrow\; \sigma_x\big|_{y=0} = \mathrm{Re}\{Z\}\big|_{y=0} \tag{2.5}$$

$$\sigma_{x,reg}\big|_{y=0} = \mathrm{Re}\{Z_{reg}\}\big|_{y=0} = -\frac{P}{\pi}\frac{\sqrt{x'-a}}{(x'-x_0)\sqrt{a-x_0}}\,,\; x' > a \tag{2.6}$$

In eq.(2.6) x' is the x-value at which the constant σ_x-stress term is evaluated. The regular x-stress at $x' = a$ is then given by

$$\sigma_{x,reg}\big|_{x\to 0} = -\frac{P}{\pi}\lim_{x'\to a}\frac{\sqrt{x'-a}}{(x'-x_0)\sqrt{a-x_0}} \tag{2.7}$$

and the Green's function reads

$$\Rightarrow \qquad t_0 = -\frac{1}{\pi}\lim_{x'\to a}\frac{\sqrt{x'-a}}{(x'-x_0)\sqrt{a-x_0}}\,. \tag{2.8}$$

From (2.8), the T-stress can be derived for a couple of forces acting on a semi-infinite crack in an infinite body, namely,

$$T = t_0 = \begin{cases} 0 & \text{for } x < a \\ -\infty & \text{for } x = a \end{cases} . \tag{2.9}$$

Crack loading σ_y is represented by a Taylor series with respect to the crack tip

$$\sigma_y(x) = \sigma_y\big|_{x=a} - \frac{d\sigma_y}{dx}\bigg|_{x=a} (a-x) + \frac{1}{2}\frac{d^2\sigma_y}{dx^2}\bigg|_{x=a} (a-x)^2 - +... \tag{2.10}$$

The corresponding T-stress contribution resulting from the asymptotic part of Green's function reads after replacing x_0 by x (see also [6])

$$T = \int_0^a t_0(x', a, x)\, \sigma(x) dx = -\frac{1}{\pi}\sigma_y\big|_{x=a} \lim_{x'\to a}\sqrt{x'-a}\int_0^a \frac{dx}{(x'-x)\sqrt{a-x}} \tag{2.11}$$

$$= -\frac{1}{\pi}\sigma_y\big|_{x=a} \lim_{x'\to a}\sqrt{x'-a}\left[\frac{2}{\sqrt{x'-a}} \arctan\sqrt{\frac{x'-a}{a-x}}\right]_0^a =$$

$$= -\frac{1}{\pi}\sigma_y\big|_{x=a} \lim_{x'\to a}\left[\pi - \arctan\sqrt{\frac{x'-a}{a}}\right] = -\sigma_y\big|_{x=a} \tag{2.12}$$

Since the two relations

$$T = t_0 = \begin{cases} 0 & \text{for } x < a \\ -\infty & \text{for } x = a \end{cases} , \qquad T = \int_0^a t_0\, \sigma(x)\, dx = -\sigma_y\big|_{x=a} \tag{2.13}$$

are identical with the definitions of the Dirac δ-function, we can finally write

$$t_0 = -\delta(a-x) \tag{2.14}$$

Introducing this in (2.1) yields

$$T = -\sigma_y\big|_{x=a} + \int_0^a t_{reg}\, \sigma(x)\, dx \tag{2.15}$$

If a σ_x stress component exists at the location of the tip of the prospective crack in the uncracked body, the total T-value is obtained by adding this stress contribution, i.e.

$$T = \sigma_x\big|_{x=a} - \sigma_y\big|_{x=a} + \int_0^a t_{reg}\ \sigma(x)\, dx \tag{2.16}$$

2.2 Power series representation of Green's function

Following the analysis of Sham (eq.(32) in [3]), the *T*-stress contribution given by the integrals in (2.15) or (2.16) can be expressed as

$$\int_0^a t_{reg}\ \sigma(x)\, dx \propto \tfrac{1}{\pi} \int_{Crack\ area} [X(s)u_r + Y(s)v_r]ds \tag{2.17}$$

for crack face loading (extending over the upper and lower crack surface) with tractions *X* and *Y* acting in x- and y- direction.

The relevant displacement in the surroundings of a crack reads

$$\frac{u}{\sigma * W} = \frac{1+\nu}{E}\sum_{n=0}^{\infty} A_n \left(\frac{r}{W}\right)^{n+1/2} \frac{2n+3}{2n-1}[(n+4\nu-\tfrac{5}{2})\cos(n-\tfrac{1}{2})\varphi - (n-\tfrac{1}{2})\cos(n+\tfrac{3}{2})\varphi] +$$

$$+\frac{1+\nu}{E}\sum_{n=0}^{\infty} A^*_n \left(\frac{r}{W}\right)^{n+1} [(n+4\nu-2)\cos n\varphi - (n+2)\cos(n+2)\varphi] \tag{2.18}$$

$$\frac{v}{\sigma * W} = \frac{1+\nu}{E}\sum_{n=0}^{\infty} A_n \left(\frac{r}{W}\right)^{n+1/2} \frac{2n+3}{2n-1}[(n-\tfrac{1}{2})\sin(n+\tfrac{3}{2})\varphi - (n-4\nu+\tfrac{7}{2})\sin(n-\tfrac{1}{2})\varphi] +$$

$$+\frac{1+\nu}{E}\sum_{n=0}^{\infty} A^*_n \left(\frac{r}{W}\right)^{n+1} [(n+2)\sin(n+2)\varphi - (n-4\nu+4)\sin n\varphi] \tag{2.19}$$

In the following considerations, the tractions *Y*(*s*) normal to the crack surface are of interest exclusively. Therefore, it is set *X*(*s*)=0.

The relevant crack face displacements result by taking φ=±π as

$$\frac{v_r}{\sigma * W} = \frac{1+\nu}{E}\sum_{n=0}^{\infty} A_n \left(\frac{r}{W}\right)^{n+1/2} \frac{2n+3}{2n-1} 4(\nu-1) \tag{2.20}$$

From (2.17), it can be concluded that

$$\int_0^a t_{reg}\ \sigma_y(x)\, dx \propto \int_{Crack} [X(s)u_r + Y(s)v_r]ds \propto \int_{Crack} Y(s)v_r ds \propto \int_0^a \sigma_y(x)\, v_r\, dx \tag{2.21}$$

The Green's or weight function is the T-stress caused by a point force P at location x of the 2-dimensional specimen or a line load in thickness direction P/B (for the 3-dimensional case) with

$$\sigma_y(x') = P\delta(x - x') \tag{2.22}$$

Insertion of (2.22) into (2.21) and use of the well-known properties of the Dirac delta function δ results in

$$t_{reg}(x) \propto v_r(x) \tag{2.23}$$

and with (2.20) a power series expansion for the Green's function is obtained as

$$t_{reg}(x) = \sum_{n=0}^{\infty} C_n (a - x)^{n+1/2} \tag{2.24}$$

By applying the finite element method, the first coefficients C_0 were determined for several crack geometries. Crack elements very close to the tip were loaded with a constant crack face pressure. The T-stress was determined for a large number of contours and is plotted in Fig. 2.2a versus the contour number. The plateau values represent the T-stress. These values are plotted in Fig. 2.2b as a function of the size d of the loaded crack surface. From this plot and Fig. 2.2c, the following expressions are obtained for the DCB specimen

$$T / p_0 = 0.747(d / h)^{3/2} \tag{2.25}$$

and for the edge crack in a large plate (Fig. 2.2d)

$$T / p_0 = 0.199(d / a)^{3/2} \tag{2.26}$$

Figure 2.2e shows the results for the standard compact tension (CT) specimen.

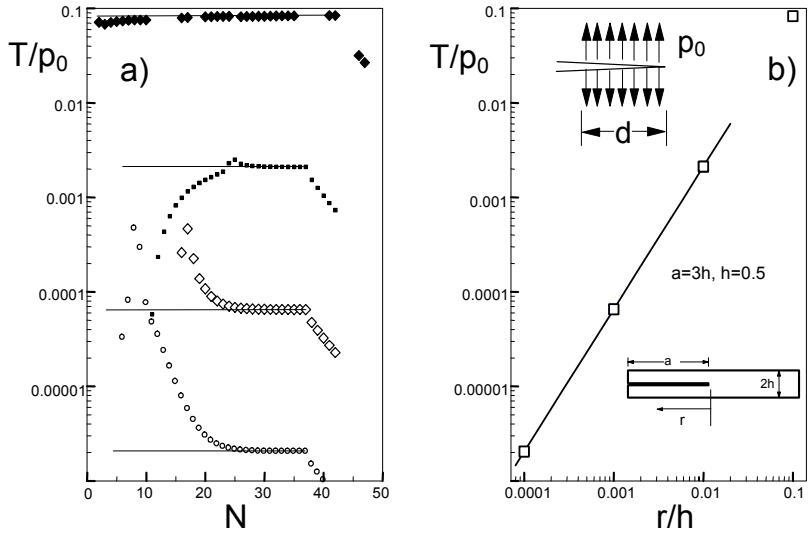

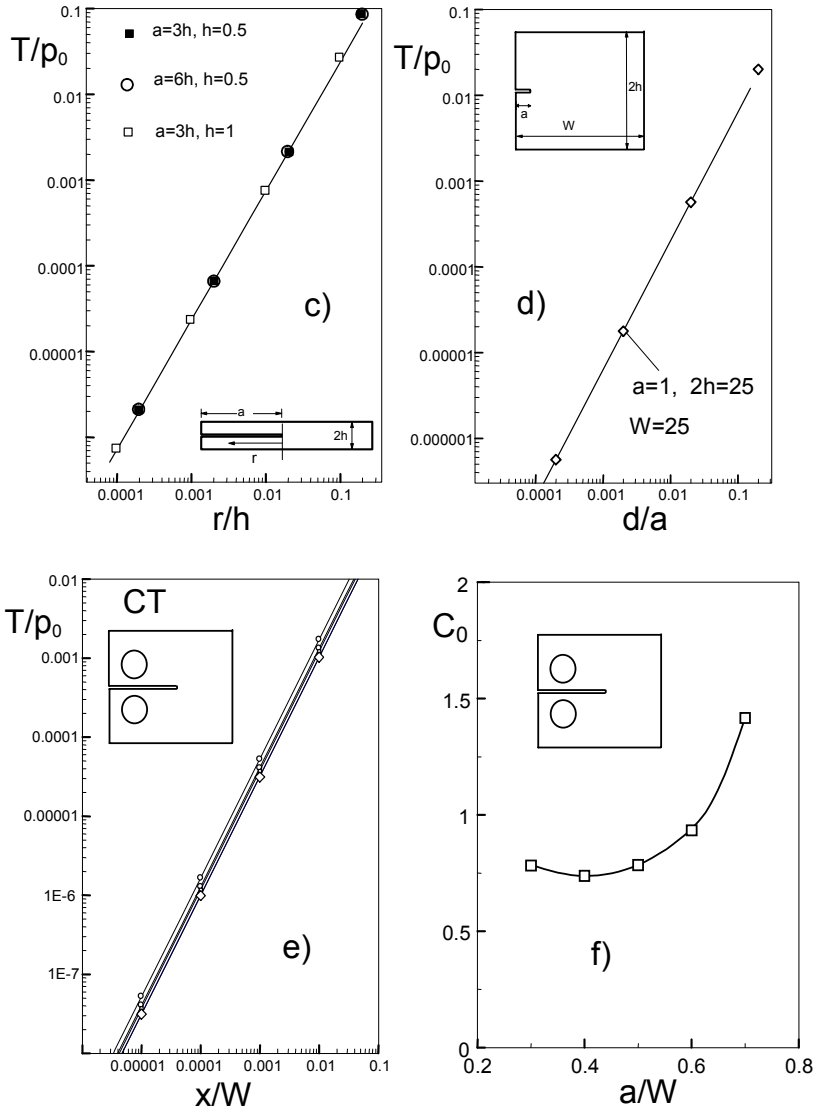

Fig. 2.2 T-stress for near-tip loading by a constant pressure p_0. a) T-stress for a DCB specimen versus number of contours, b) plateau values of Fig. 2.2a versus size of the loading region c) results for DCB specimens with different heights h, d) results for a small crack of a=1 in a large body of H=12.5 and W=25, e) results for the standard CT specimen, f) first coefficient C_0 as a function of a/W.

All these results allow to determine the first coefficient of the power series representation. It results from (2.16) and (2.24) that

$$T / p_0 = \int_0^d C_0 \sqrt{r}\, dr = \tfrac{2}{3} C_0 d^{3/2} \tag{2.27}$$

By comparing the coefficients of the $d^{3/2}$ dependency of (2.25) and (2.26) with (2.27), we obtain $C_0 \cong 9/8$ for the DCB specimen and C_0=0.3 for the edge crack in the half-space. In the case of the CT specimen, the coefficient C_0 depends on the relative crack length a/W, as shown in Fig. 2.2f.

2.3 Approximate Green's function representation by polynomials

The Green's function expressed by a power series, eq.(2.23) is exact, but unfortunately only a few coefficients C_n can be determined in many cases. If a reduced precision is allowed, a polynomial representation can be chosen.

Different types of setup have been used so far. In [8], a truncated power series was proposed

$$t = t_0 + \sum_{n=0}^{N} C_n (1 - x/a)^{n+\frac{1}{2}} \tag{2.28}$$

and successfully applied by Wang [7].

A second setup with integer exponents was also proposed in [8]. If assuming that the difference between the complete Green's function $t(b)$ and its asymptotic part $t_0(b)$ can be expressed by a Taylor series for $b=a-x\to 0$

$$t_{corr}(b) = t(b) - t_0(b) = f(b) = 0 + \left.\frac{\partial t}{\partial b}\right|_{b=0} b + \tfrac{1}{2}\left.\frac{\partial t^2}{\partial b^2}\right|_{b=0} b^2 + \ldots \tag{2.29}$$

the complete Green's function can be written as

$$t = t_0 + \sum_{n=1}^{\infty} D_n (1 - x/a)^n \tag{2.30}$$

By restricting the expansion to the leading term, the approximation

$$t \cong \delta(a-x) + C\left(1 - \frac{x}{a}\right), \quad \Rightarrow \quad T = -\sigma_y\,|_{x=a} + C\int_0^a (1 - x/a)\,\sigma_y\,\mathrm{d}x \tag{2.31}$$

is obtained. A simple procedure to determine approximate Green's functions is to determine the unknown coefficients in the series representation (2.30) for known T-solutions of reference loading cases [8]. If, for example, the T-term of an edge-cracked plate under pure crack-face pressure p_0 is known, insertion of (2.29) into eq.(2.1) yields

$$T_t = p_0\int_0^a t(x,a)dx = p_0\int_0^a t_0\,dx + p_0 C\int_0^a (1 - x/a)dx = p_0\left(-1 + C\frac{a}{2}\right) \tag{2.32}$$

and the coefficient C results as

$$C = \frac{2}{a}\left(1 + \frac{T_t}{p_0}\right) \tag{2.33}$$

Knowledge of additional reference solutions for T allows to determine further coefficients.

3. Edge crack in a semi-infinite body

Figure 3.1 shows an edge crack of length a in a semi-infinite body loaded by a pair of normal forces P at a distance x from the crack mouth.

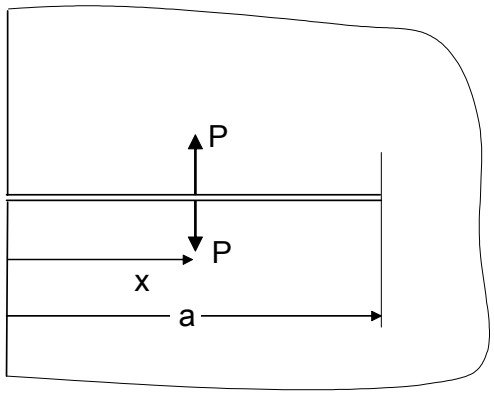

Fig. 3.1 Edge-cracked half space.

The Green's function for the stress intensity factor K_I and the T-stress of a crack of length a were computed by finite elements. A body of height 200a and width 200a was chosen for this purpose. Figure 3.2 shows the stress intensity factor and the T-stress as circles. The stress intensity factor for this load, called the weight function, is well known and can be expressed by [8]

$$h = \sqrt{\frac{2}{\pi a}}\left(\frac{1}{\sqrt{1-x/a}} + \sum_{n=0}^{5} D_n (1-x/a)^{n+1/2} \right) \tag{3.1}$$

with the coefficients D_n compiled in Table 3.1.

n	D_n	n	D_n
0	0.568852	3	0.227211
1	0.031854	4	-0.828528
2	0.463397	5	0.351383

Table 3.1 Coefficients for the weight function eq.(3.1).

This weight function is identical for mode-II and mode-I loading. It is introduced in Fig. 3.2a as a curve.

The T-stress is shown in Fig. 3.2b. This dependency can be represented by the relation of

$$\frac{T}{P/(Ba)} = 0.3447\sqrt{1-x/a} + 0.0867(1-x/a)^{3/2} + 0.7329(1-x/a)^{5/2} \tag{3.2}$$

This relation is entered in Fig. 3b as a curve.

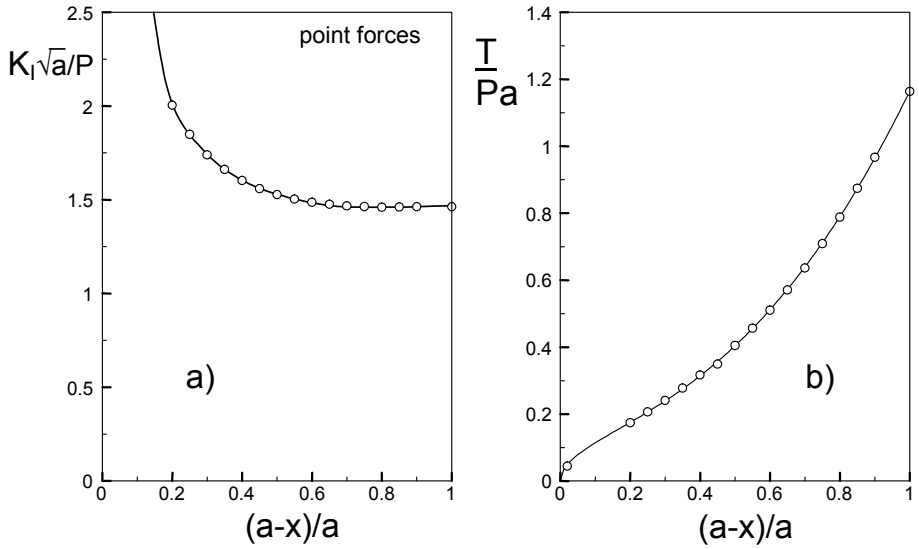

Fig. 3.2 a) Stress intensity factor and T-stress for point forces, b) Green's function for the T-stress.

4. Double cantilever beam (DCB)

The double-cantilever-beam (DCB) specimen is shown in Fig. 4.1. A line load P/B (B= specimen thickness, here chosen as B=1) is applied at a distance (a-x) from the crack tip normally to the crack face.

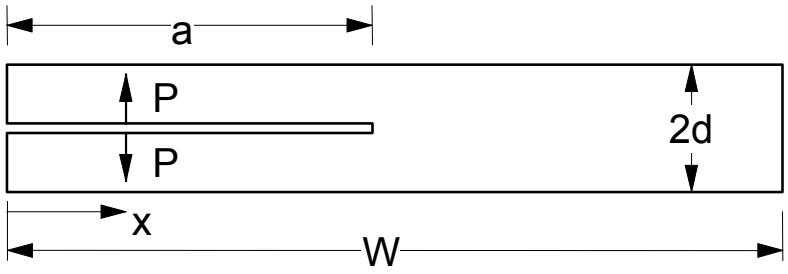

Fig. 4.1 Double cantilever beam specimen under crack-face loading by line load P.

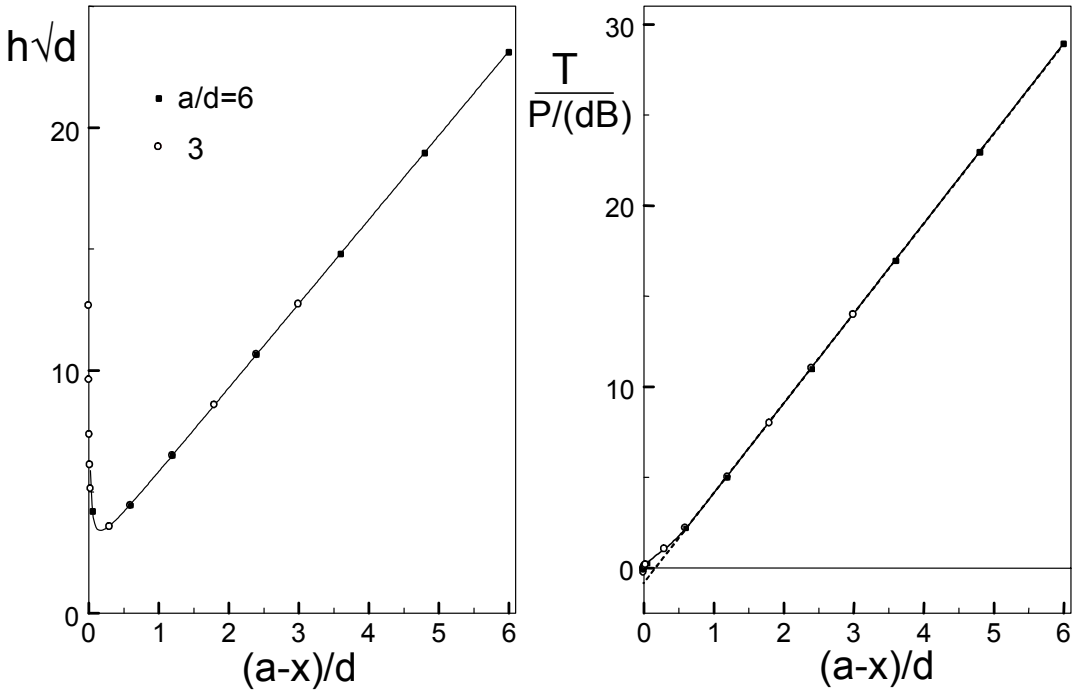

Fig. 4.2 a) Weight function for stress intensity factors, b) Green's function for T-stress

The weight function is given in [8] as

$$h = \sqrt{\frac{12}{d}}\left(\frac{a-x}{d} + 0.68\right) + \sqrt{\frac{2}{\pi(a-x)}}\exp\left(-\sqrt{12\frac{a-x}{d}}\right) \tag{4.1}$$

and introduced in Fig. 4.2a as the curve. Its agreement with the FE results is excellent. The T-stress results are shown in Fig. 4.2b. The asymptotic solutions for $(a\text{-}x)/d>0$ can be expressed by

$$\frac{T}{P/(Bd)}=\begin{cases}4.95\dfrac{a-x}{d}-0.9 & for\ \ (a-x)/d>1\\ 0.3\sqrt{\dfrac{a-x}{d}} & for\ \ (a-x)/d\to 0\end{cases} \tag{4.2}$$

This relation is represented by the dashed line. A relation for any $(a\text{-}x)/d>0$ reads

$$\frac{T}{P/(Bd)}=\lambda\left(\tfrac{9}{8}\sqrt{\frac{a-x}{d}}+\tfrac{5}{2}\left(\frac{a-x}{d}\right)^{3/2}\right)+(1-\lambda)\left(4.95\frac{a-x}{d}-0.9\right)-\delta(a-x) \tag{4.3}$$

with an interpolation parameter

$$\lambda=\exp\left(-2\left(\frac{a-x}{d}\right)^{2}\right) \tag{4.4}$$

represented by the (solid curve).

5. Compact tensile (CT) specimen

Several analyses of the CT specimen were given in the literature [10-13]. Under slightly modified boundary conditions, rather strong differences were found especially for short crack lengths.

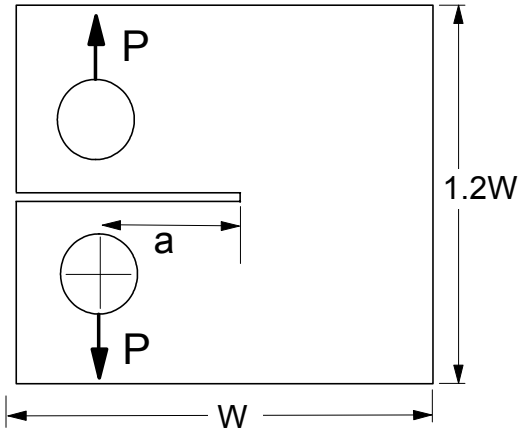

Fig. 5.1 Compact tension specimen.

A stress intensity factor solution for the standard CT specimens was proposed by Newman [14] and Srawley [15]

$$K_I = \frac{P}{B\sqrt{W}} \frac{(2+\alpha)(0.886+4.64\alpha-13.32\alpha^2+14.72\alpha^3-5.6\alpha^4}{(1-\alpha)^{3/2}} \tag{5.1}$$

with $\alpha=a/W$. Literature results for the biaxiality ratio β

$$\beta = \frac{T\sqrt{\pi a}}{K} \tag{5.2}$$

proposed by Leevers and Radon [11] are entered in Fig. 5.2a together with the limit case $\alpha \rightarrow 1$ taken from [6]. The curve plotted in Fig. 5.2a can be described by

$$\beta = \frac{-0.2+2.0307\ \alpha+0.675\ \alpha^2-7.4756\ \alpha^3+6.349\ \alpha^4-1.0772\ \alpha^5}{\sqrt{1-\alpha}} \tag{5.3}$$

The T-stress term results from eqs.(5.1)-(5.3). In this context, it has to be noted that the results in Fig. 5.2a were not derived for the standard CT specimen with large holes. In reference [11], the T-stress was determined by applying of shear tractions along the loading line and by application of point forces in the centres of fictitious holes. In our study, we modelled the test specimen according to ASTM E399 and considered point forces to be active at the contact

points. The results are plotted in Fig. 5.2b. Based on these results, it is recommended to use cracks with α>0.25.

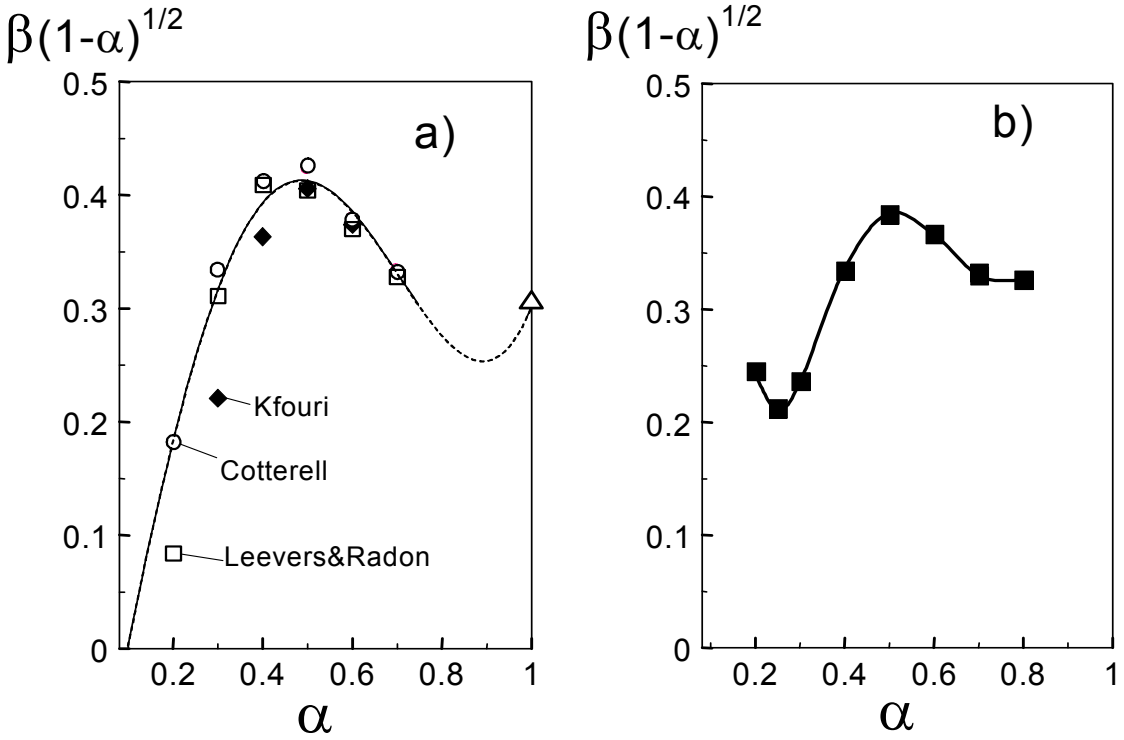

Fig. 5.2 a) Biaxiality ratio of the CT specimen from literature; curve: eq.(5.3), squares: Leevers and Radon [11], circles: Cotterell [12], diamond squares: Kfouri [10], triangle: limit case from [6], b) biaxiality ratio for a standard CT specimen.

For the crack length region $0.4 \le a/W \le 0.6$, the T-stress is given by

$$\frac{T}{BW} = -0.57 + 4.145\alpha + 10.65\alpha^2 \qquad (5.4)$$

6. Oblique edge crack

A slant edge crack in a semi-infinite body including an angle φ with the x-axis, is illustrated in Fig. 6.1. The stress intensity factors and the T-stress term are compiled in Table 6.1 for a remote stress in y-direction and in Table 6.2 for a constant stress in x-direction. Table 6.3 contains these parameters for a constant pressure *p* acting on the crack faces. The results of Table 6.3 reflect the well-known feature that the fracture mechanics parameters for crack-face pressure are identical with the sum of parameters under $\sigma_x=\sigma_y$ loading. The geometric functions are defined by

$$K_I = \sigma F_I \sqrt{\pi a}\ , \quad K_{II} = \sigma F_{II} \sqrt{\pi a} \tag{6.1}$$

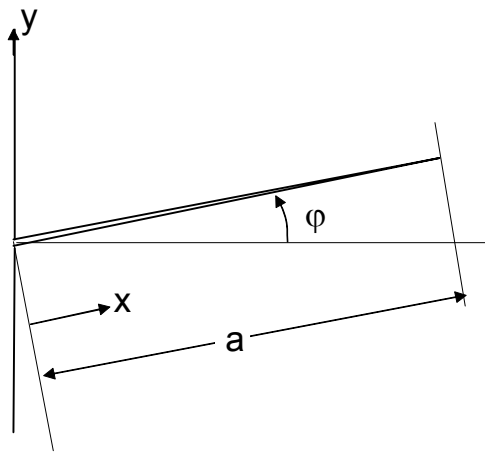

Fig. 6.1 Oblique edge crack.

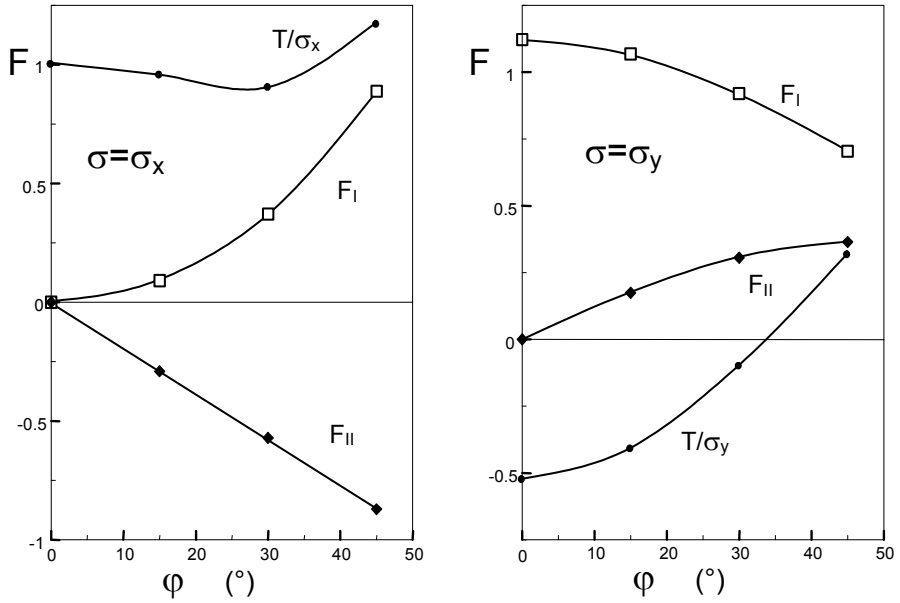

Fig. 6.2 Mixed-mode stress intensity factors and T stress; a) constant stresses in x-direction, b) remote stresses in y-direction.

φ (°)	$K_I / \sigma_x \sqrt{a\pi}$	$K_{II} / \sigma_x \sqrt{a\pi}$	T / σ_x
0	0	0	1
15	0.0912	-0.291	0.9545
30	0.372	-0.571	0.9026
45	0.888	-0.871	1.169

Table 6.1 Stress intensity factors and T-stress under constant x-stresses.

φ (°)	$K_I / \sigma_y \sqrt{a\pi}$	$K_{II} / \sigma_y \sqrt{a\pi}$	T / σ_y
0	1.1215	0	-0.526
15	1.069	0.174	-0.411
30	0.920	0.306	-0.1013
45	0.705	0.365	0.3153

Table 6.2 Stress intensity factors and T-stress under remote y-stresses.

φ (°)	$K_I / p\sqrt{a\pi}$	$K_{II} / p\sqrt{a\pi}$	T / p
0	1.1215	0	0.474
15	1.159	-0.117	0.544
30	1.291	-0.265	0.804
45	1.592	-0.506	1.484

Table 6.3 Stress intensity factors and T-stress under constant pressure on crack faces.

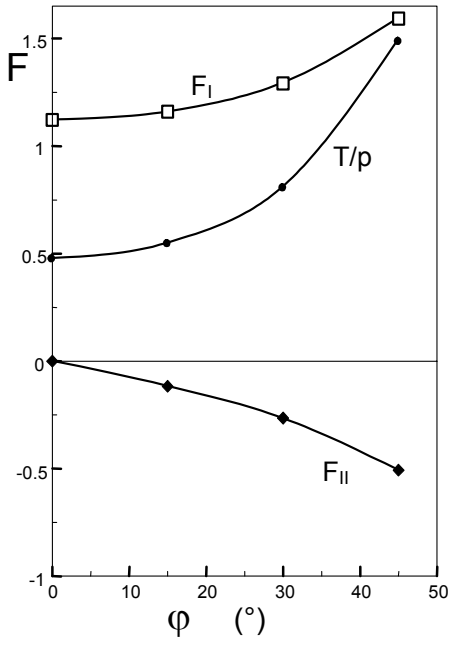

Fig. 6.3 Mixed-mode stress intensity factors and T-stress for constant crack face pressure *p*.

Under a combined crack-face loading, the stress intensity factors for edge cracks generally read

$$K_I = \int_0^a [h_I^{(1)}(x,a)\sigma_n(x) + h_I^{(2)}(x,a)\tau(x)]dx \tag{6.2}$$

$$K_{II} = \int_0^a [h_{II}^{(1)}(x,a)\sigma_n(x) + h_{II}^{(2)}(x,a)\tau(x)]dx \tag{6.3}$$

defining 4 weight functions [8]. The stress intensity factors under point forces directly provide the weight functions. For a three-terms approximation of the weight function $h_{II}^{(1)}$

$$h_{II}^{(1)} = \sqrt{\frac{2}{\pi a}}\left(A_1\sqrt{1-x/a} + A_2(1-x/a)^{3/2} + A_3(1-x/a)^{5/2}\right) \tag{6.4}$$

the coefficients are compiled in Table 6.4

φ (°)	A_1	A_2	A_3
15	-0.1890	-0.3011	-0.0427
30	-0.4053	-0.7803	-0.0211
45	-0.6901	-1.8071	+0.2039

Table 6.4 Weight function coefficients according to eq.(6.4).

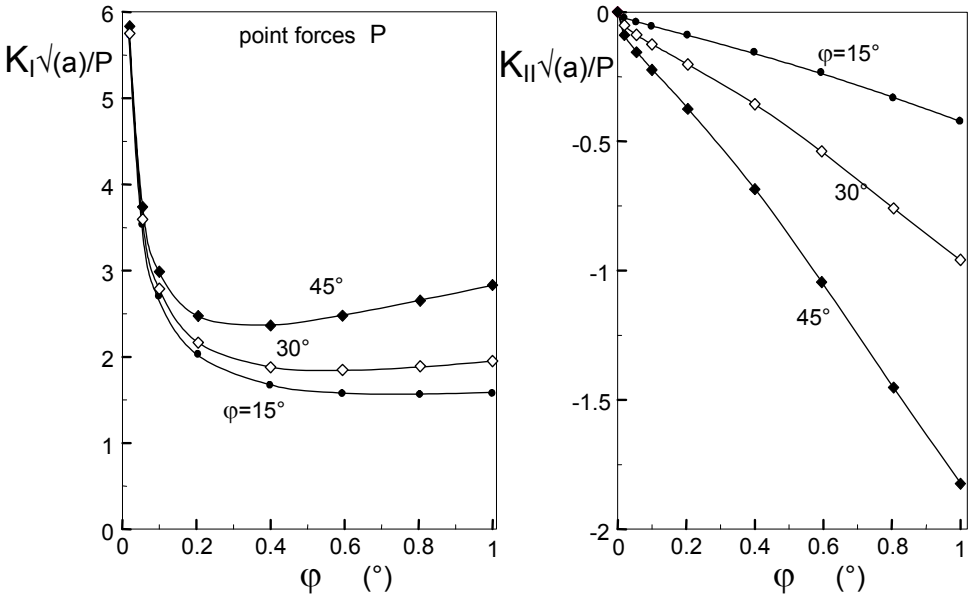

Fig. 6.4 Mixed-mode stress intensity factors for point forces P.

For small angles φ, the weight function can be approximated by

$$h_{II}^{(1)} \cong -\sqrt{\frac{2}{\pi a}}\left(0.7053\sqrt{1-x/a} + 1.124(1-x/a)^{3/2} + 0.1593(1-x/a)^{5/2}\right)\sin\varphi \tag{6.5}$$

7. Kink edge crack

The edge crack with a kink is illustrated in Fig. 7.1. Stress intensity factors and T-stress were computed for constant stresses in y- and x- direction and for a constant pressure p on the crack faces. The results are compiled in Tables 7.1-7.3 and Fig. 7.2. The results of Table 7.3 also reflect the well-known feature that the fracture mechanics parameters for crack-face pressure are identical with the sum of parameters under $\sigma_x=\sigma_y$ loading. The Tables 7.1-7.3 also contain the results of Tables 6.1-6.3, which correspond to a kink crack with $c_1/a=0$, $c_2/a=1$.

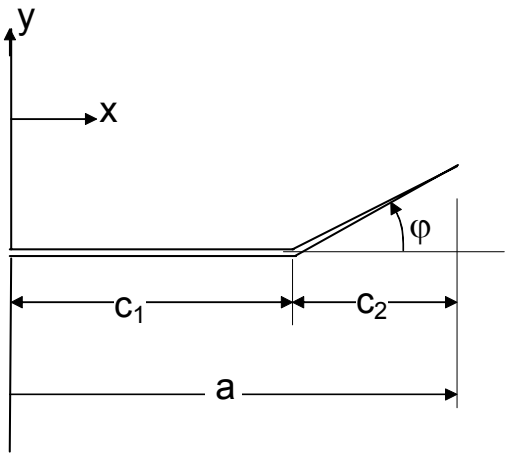

Fig. 7.1 Kinked edge crack.

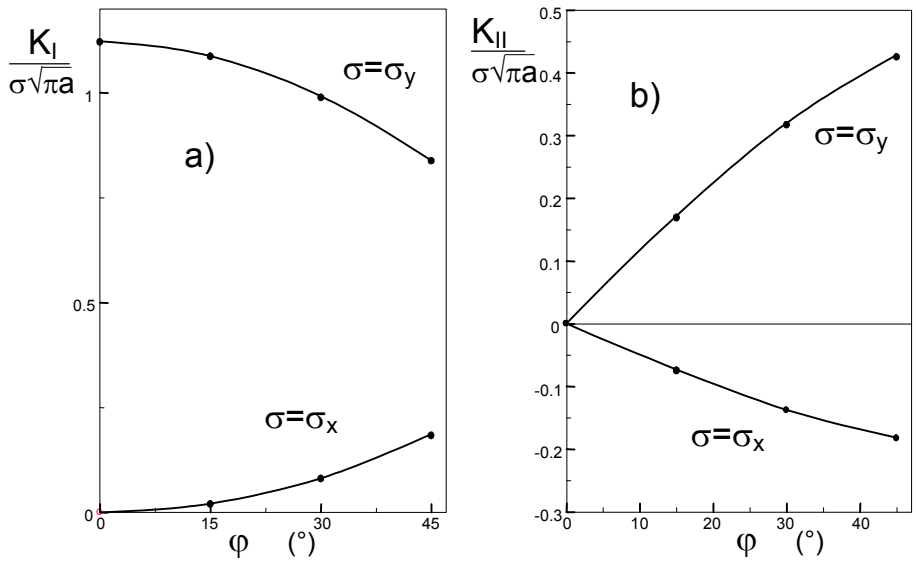

Fig. 7.2 Stress intensity factors for $c_1/a=0.9$ under loading in x and y- direction.

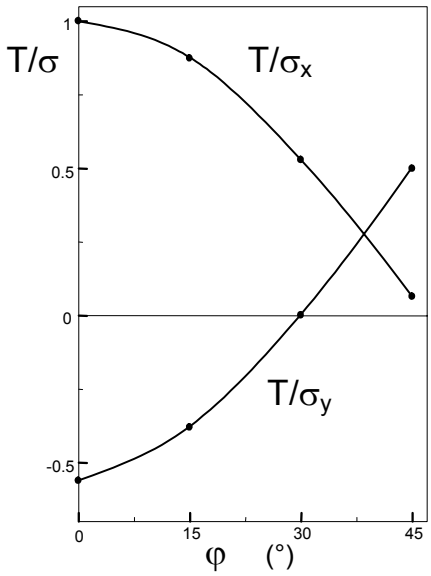

Fig. 7.3 T-stress for c_1/a=0.9 under loading in x and y- direction.

c_1/a	c_2/a	φ (°)	$K_I / \sigma_x \sqrt{a\pi}$	$K_{II} / \sigma_x \sqrt{a\pi}$	T / σ_x
		0	0	0	1
0	1	15	0.0912	-0.291	0.9545
0	1	30	0.372	-0.571	0.9026
0	1	45	0.888	-0.871	1.169
0.9	0.1	15	0.0203	-0.0742	0.8732
0.9	0.1	30	0.0810	-0.1380	0.5284
0.9	0.1	45	0.1838	-0.1831	0.0636
0.95	0.05	15	0.0140	-0.0519	0.8730
0.95	0.05	30	0.0559	-0.0964	0.5284
0.95	0.05	45	0.1258	-0.1273	0.0628
0.97	0.03	15	0.0108	-0.0401	0.8731
0.97	0.03	30	0.0428	-0.0744	0.5288
0.97	0.03	45	0.0961	-0.0980	0.0643
1	0	15	0	0	
1	0	30	0	0	
1	0	45	0	0	

Table 7.1 Stress intensity factors and T-stress under constant x-stresses.

In order to check the accuracy, the finite element results were compared with the highly precise results of Noda and Oda [16] obtained by using the body force method. In Table 7.4, our

results are compared with those of [16] for c_1/a=0.1 and loading in y-direction. Maximum deviations are less than 0.25%.

c_1/a	c_2/a	φ (°)	$K_I / \sigma_y \sqrt{a\pi}$	$K_{II} / \sigma_y \sqrt{a\pi}$	T / σ_y
		0	1.1215	0	-0.526
0	1	15	1.069	0.174	-0.526
0	1	30	0.920	0.306	-0.411
0	1	45	0.705	0.365	-0.1013
0.9	0.1	15	1.087	0.1696	-0.3805
0.9	0.1	30	0.989	0.3172	0.0002
0.9	0.1	45	0.838	0.4255	0.4985
0.95	0.05	15	1.061	0.1625	-0.3506
0.95	0.05	30	0.967	0.304	0.1132
0.95	0.05	45	0.824	0.4044	0.6999
0.97	0.03	15	1.050	0.159	-0.4415
0.97	0.03	30	0.960	0.294	0.2309
0.97	0.03	45	0.820	0.3918	0.9231
1	0	15	1.093	0.1437	
1	0	30	1.011	0.2695	
1	0	45	0.887	0.3626	

Table 7.2 Stress intensity factors and T-stress under remote y-stresses.

c_1/a	c_2/a	φ (°)	$K_I / p\sqrt{a\pi}$	$K_{II} / p\sqrt{a\pi}$	T / p
		0	1.1215	0	0.474
0	1	15	1.159	-0.117	0.544
0	1	30	1.291	-0.265	0.804
0	1	45	1.592	-0.506	1.484
0.9	0.1	15	1.108	0.0951	0.4926
0.9	0.1	30	1.070	0.1792	0.5309
0.9	0.1	45	1.022	0.2424	0.5616
0.95	0.05	15	1.075	0.1086	0.5226
0.95	0.05	30	1.023	0.2045	0.6418
0.95	0.05	45	0.950	0.2771	0.7630
1	0	15	1.093	0.1437	
1	0	30	1.011	0.2695	
1	0	45	0.887	0.3626	

Table 7.3 Stress intensity factors and T-stress under constant internal pressure p.

φ (°)	$K_I / \sigma_y \sqrt{a\pi}$	$K_{II} / \sigma_y \sqrt{a\pi}$	$K_I / \sigma_y \sqrt{a\pi}$ [16]	$K_{II} / \sigma_y \sqrt{a\pi}$ [16]
15	1.087	0.1693	1.087	0.170
30	0.989	0.3172	0.990	0.317
45	0.839	0.4255	0.841	0.426

Table 7.4 Comparison of stress intensity factors from finite element computations with data of Noda and Oda [16] for c_2/a=0.1.

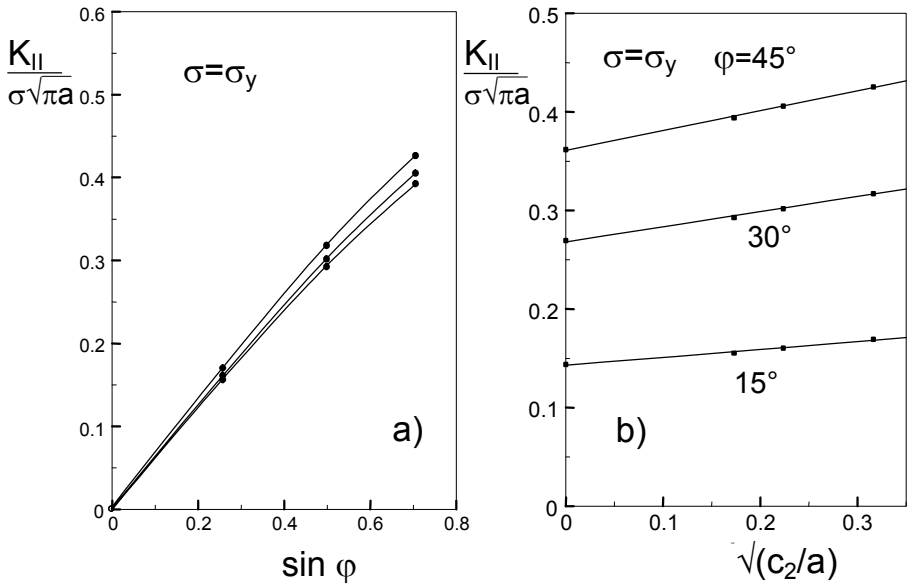

Fig. 7.4 Influence of kink length and angle on the mode-II stress intensity factor for $\sigma=\sigma_y$.

In Fig. 7.4 the mode-II stress intensity factors for remote stress in y-direction are plotted as a function of the sine of the angle φ and the square root of the parameter c_2/a. Figure 7.5 represents the data for constant stress in x-direction and Fig. 7.6 for constant crack-face pressure p. The values for c_2/a=0 in Fig. 7.4 were obtained from the limit case of a small kink crack ahead of a semi-infinite crack in an infinite body that is loaded by a mode-I contribution, exclusively. If $\overline{K}_I$ is the mode-I stress intensity factor for the straight crack, the mode-II stress intensity factor for the kink crack is then given as

$$K_{II} = C_{21}(\varphi)\overline{K}_I \tag{7.1}$$

$$\overline{K}_I = F\,\sigma_y \sqrt{\pi a} \tag{7.2}$$

with coefficient C_{21} reported by Isida and Nishino [17]. In the case of an *edge crack*, the geometric function F=1.1215 differs from the case of the semi-infinite crack (where F=1).
For small angles φ and c_2<<a, the data shown in Figs. 7.4-7.6 can be expressed by the following approximations:

$\sigma=\sigma_y$:

$$\frac{K_{II}}{\sigma_y\sqrt{\pi a}} = 1.1215\sin(\varphi/2)\cos^2(\varphi/2) + 0.2168\sin\tfrac{3}{2}\varphi\sqrt{\frac{c_2}{a}} \tag{7.3}$$

$\sigma=\sigma_x$:

$$\frac{K_{II}}{\sigma_x\sqrt{\pi a}} \cong -\frac{\sqrt{8}}{\pi}\sin\varphi\cos^{1/2}\varphi\sqrt{c_2/a} - 0.204\frac{c_2}{a}\varphi^2 \tag{7.4}$$

crack-face pressure p:

$$\frac{K_{II}}{p\sqrt{\pi a}} = 1.1215\sin(\varphi/2)\cos^2(\varphi/2) - 0.399\sin\tfrac{3}{2}\varphi\sqrt{\frac{c_2}{a}} \tag{7.5}$$

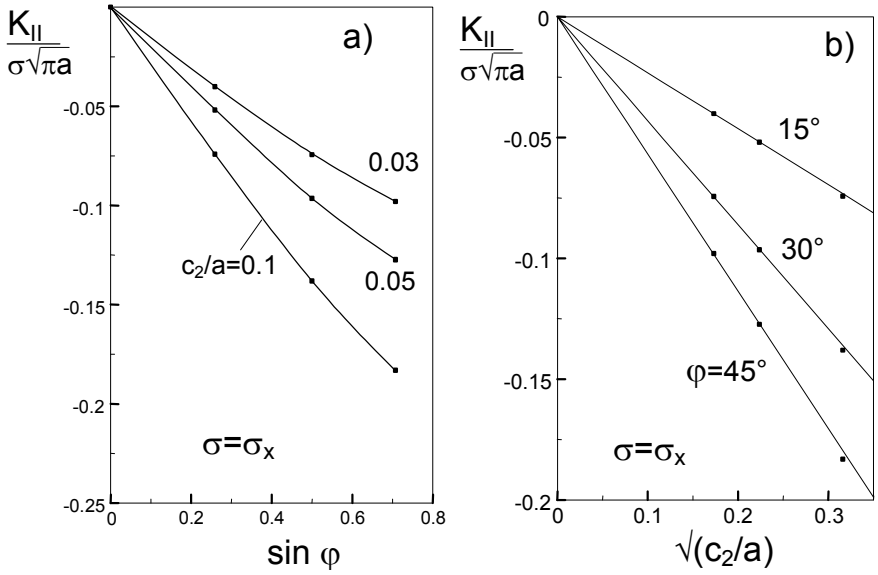

Fig. 7.5 Influence of kink length and angle on the mode-II stress intensity factor for $\sigma=\sigma_x$.

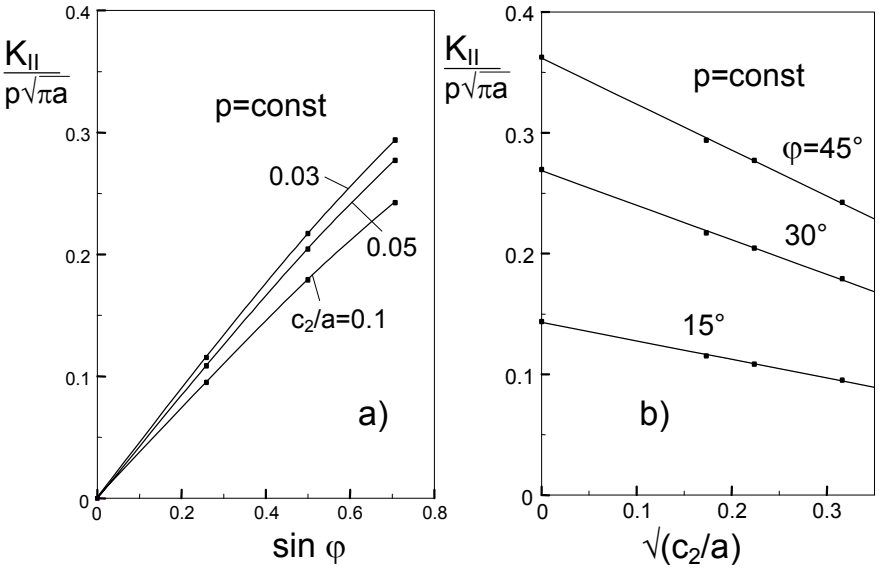

Fig. 7.6 Influence of kink length and angle on the mode-II stress intensity factor at crack-face pressure p.

8. Tetrahedron-shaped cracks

A tetrahedron-shaped crack in a plate of thickness B is shown in Fig. 8.1. By finite element computations, the Green's functions were determined for mixed-mode stress intensity factors and T-stress. Therefore, point forces P normal to the crack and Q in crack direction were applied.

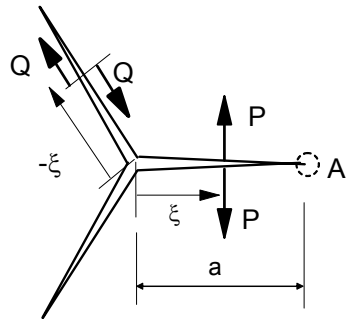

Fig. 8.1 Tetrahedron-shaped crack with normal and tangential point forces.

Under a combined crack-face loading, the stress intensity factors generally read

$$K_I = \int_{-a}^{a} [h_I^{(1)}(\xi,a)\sigma_n(\xi) + h_I^{(2)}(\xi,a)\tau(\xi)]d\xi \tag{8.1}$$

$$K_{II} = \int_{-a}^{a} [h_{II}^{(1)}(\xi,a)\sigma_n(\xi) + h_{II}^{(2)}(\xi,a)\tau(\xi)]d\xi \tag{8.2}$$

The weight function $h(\xi,a)$ can be interpreted as the Green's function for a stress intensity factor problem. This means that the weight function is identical to the stress intensity factor caused by a pair of normal forces P and Q acting at the points $\xi = \xi'$ and ξ''. If we express the single forces by stress distributions

$$\sigma(\xi) = \frac{P}{B}\delta(\xi - \xi') \; ; \quad \tau(\xi) = \frac{Q}{B}\delta(\xi - \xi'') \tag{8.3}$$

(δ = Dirac delta function), insertion of these stress distributions into eq.(8.1) yields

$$K_I = \frac{P}{B}\int_0^a h_I^{(1)}(\xi,a)\delta(\xi - \xi')\, d\xi + \frac{Q}{B}\int_0^a h_I^{(2)}(\xi,a)\delta(\xi - \xi'')\, d\xi$$

$$K_I = \frac{P}{B}h_I^{(1)}(\xi',a) + \frac{Q}{B}h_I^{(2)}(\xi'',a) \tag{8.4}$$

and in the same way, it results from eq.(8.2)

$$K_{II} = \frac{P}{B}h_{II}^{(1)}(\xi',a) + \frac{Q}{B}h_{II}^{(2)}(\xi'',a) \tag{8.5}$$

$$h_I^{(1)} = \sqrt{\frac{1+\xi/a}{\pi a}}\left[\frac{1}{\sqrt{1-\xi/a}} + A_I^{(1)}\sqrt{1-\xi/a} + B_I^{(1)}(1-\xi/a)^{3/2} + C_I^{(1)}(1-\xi/a)^{5/2}\right] \quad (8.6)$$

$$h_I^{(2)} = \sqrt{\frac{1+\xi/a}{\pi a}}\left[A_I^{(2)}\sqrt{1-\xi/a} + B_I^{(2)}(1-\xi/a)^{3/2} + C_I^{(2)}(1-\xi/a)^{5/2}\right] \quad (8.7)$$

$$h_{II}^{(1)} = \sqrt{\frac{1+\xi/a}{\pi a}}\left[A_{II}^{(1)}\sqrt{1-\xi/a} + B_{II}^{(1)}(1-\xi/a)^{3/2} + C_{II}^{(1)}(1-\xi/a)^{5/2}\right] \quad (8.8)$$

$$h_{II}^{(2)} = \sqrt{\frac{1+\xi/a}{\pi a}}\left[\frac{1}{\sqrt{1-\xi/a}} + A_{II}^{(2)}\sqrt{1-\xi/a} + B_{II}^{(2)}(1-\xi/a)^{3/2} + C_{II}^{(2)}(1-\xi/a)^{5/2}\right] \quad (8.9)$$

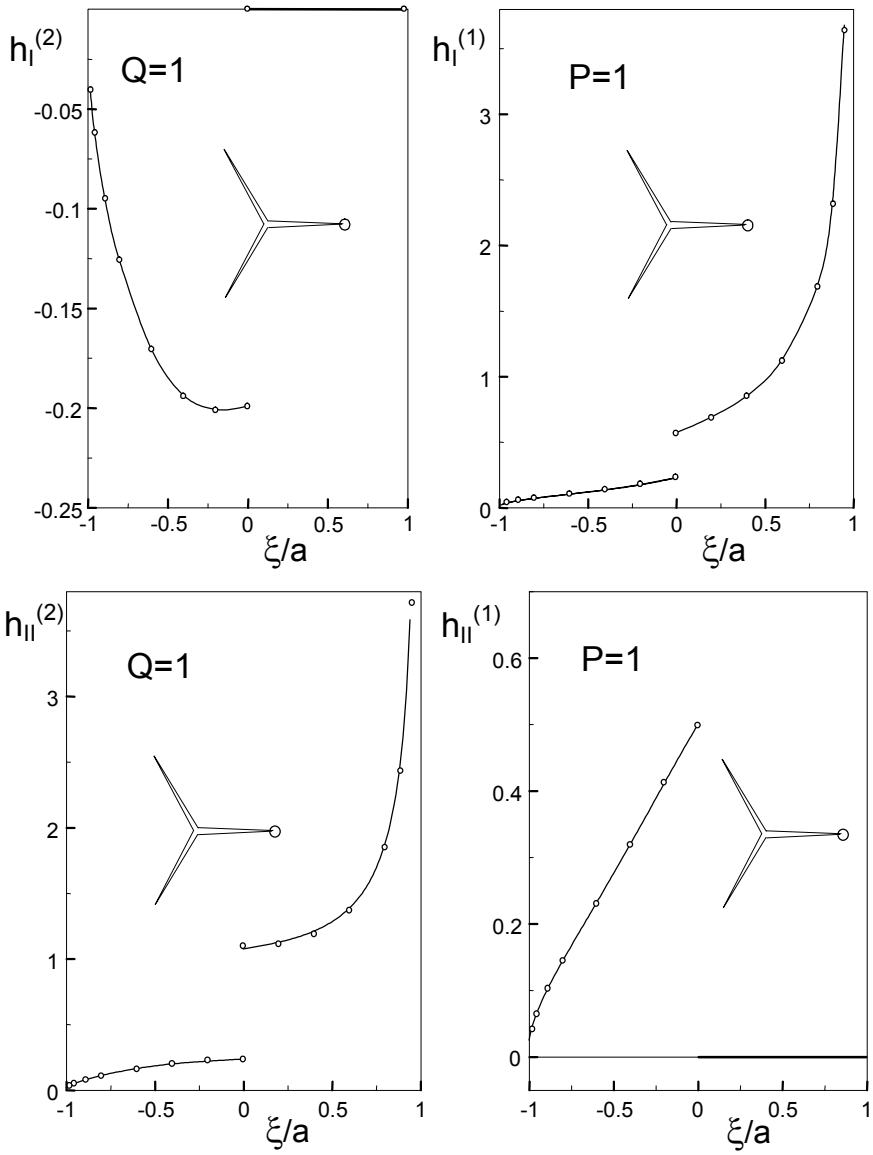

Fig. 8.2 Mixed-mode weight functions for tetrahedron-shaped cracks.

The mixed-mode stress intensity factors are shown in Fig. 8.2 and the T-stress in Fig. 8.3. The coefficients for eqs.(8.6)-(8.9) are compiled in Table 8.1. In all cases $\xi<0$, the data correspond to load on the upper crack part (as illustrated for Q in Fig. 8.1). For the lower crack part, the symmetry of K_{I} and T and antisymmetry of K_{II} have to be taken into account.

	A	B	C
$\xi<0$	$A_I^{(1)}$ =-1.125	$B_I^{(1)}$ =0.6402	$C_I^{(1)}$ =-0.1228
$\xi>0$	$A_I^{(1)}$ =-0.041	$B_I^{(1)}$ =0.0385	$C_I^{(1)}$ =0
$\xi<0$	$A_{II}^{(1)}$ =1.8822	$B_{II}^{(1)}$ =-1.2319	$C_{II}^{(1)}$ =0.2347
$\xi>0$	$A_{II}^{(1)}$ =0	$B_{II}^{(1)}$ =0	$C_{II}^{(1)}$ =0
$\xi<0$	$A_I^{(2)}$ =-0.1879	$B_I^{(2)}$ =-0.2416	$C_I^{(2)}$ =0.0773
$\xi>0$	$A_I^{(2)}$ =0	$B_I^{(2)}$ =0	$C_I^{(2)}$ =0
$\xi<0$	$A_{II}^{(2)}$ =-1.900	$B_{II}^{(2)}$ =1.8151	$C_{II}^{(2)}$ =-0.4950
$\xi>0$	$A_{II}^{(2)}$ =0.3142	$B_{II}^{(2)}$ =0.5885	$C_{II}^{(2)}$ =0

Table 8.1 Coefficients for weight functions eqs.(8.6)-(8.9).

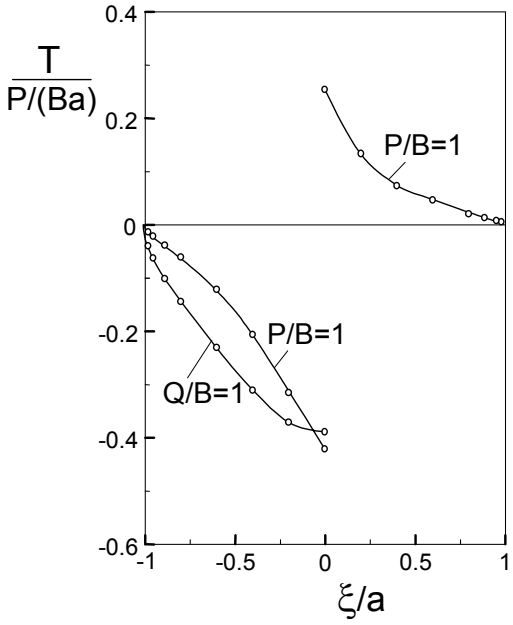

Fig. 8.3 Green's function of T-stress functions for tetrahedron-shaped cracks.

Figure 8.4 shows a modification of the tetrahedron-shaped crack with one crack part missing. The stress intensity factors are shown in Fig. 8.5

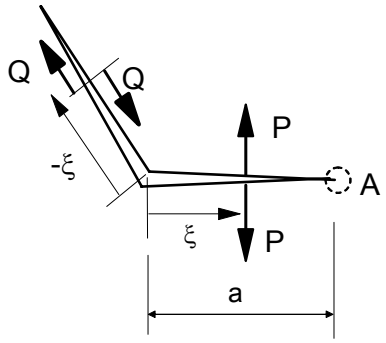

Fig. 8.4 Two cracks of equal length under an angle of 120°.

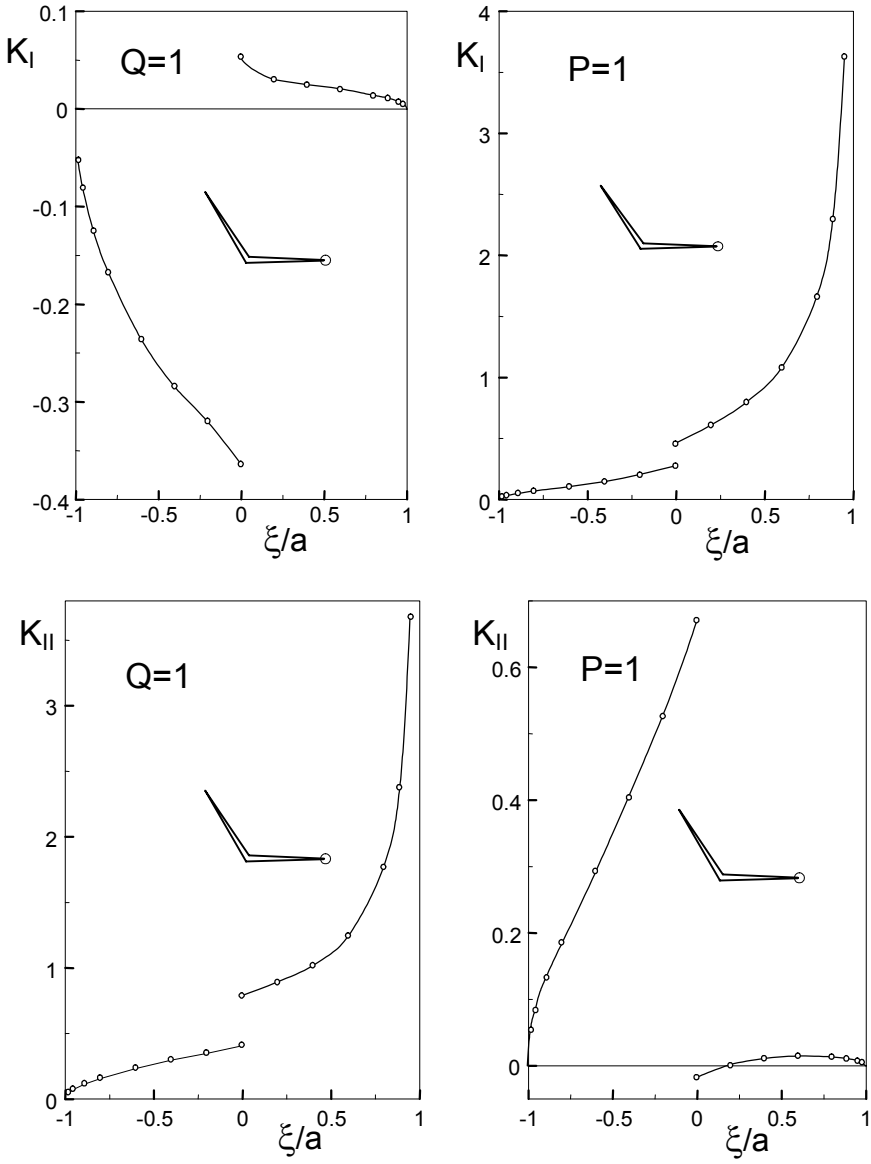

Fig. 8.5 Mixed-mode weight functions for incomplete tetrahedron-shaped cracks.

References

[1] Bückner, H., A novel principle for the computation of stress intensity factors, ZAMM **50** (1970), 529-546.

[2] Sham, T.L., The theory of higher order weight functions for linear elastic plane problems, Int. J. Solids and Struct. **25**(1989), 357-380.

[3] Sham, T.L., The determination of the elastic T-term using higher order weight functions, Int. J. Fract. **48**(1991), 81-102.

[4] Fett, T., A Green's function for T-stresses in an edge-cracked rectangular plate, Eng. Fract. Mech. **57**(1997), 365-373.

[5] Fett, T., T-stresses in rectangular plates and circular disks, Engng. Fract. Mech. **60**(1998), 631-652.

[6] Fett, T., T-stress and stress intensity factor solutions for 2-dimensional cracks, VDI-Verlag, 2002.

[7] X. Wang, Elastic *T*-stress solutions for semi-elliptical surface cracks in finite thickness plates. *Engng. Fract. Mech.* **70** (2003), pp. 731–756.

[8] Fett, T., Munz, D., Stress intensity factors and weight functions, Computational Mechanics Publications, Southampton, 1997.

[9] Irwin, G.R., Analysis of stresses and strains near the end of a crack transversing a plate, J. Appl. Mech. **24** (1957), 361-364.

[10] Kfouri, A.P., Some evaluations of the elastic T-term using Eshelby's method, Int. J. Fract. **30**(1986), 301-315.

[11] Leevers, P.S., Radon, J.C., Inherent stress biaxiality in various fracture specimen geometries, Int. J. Fract. **19**(1982), 311-325.

[12] Cotterell, B., On the fracture path stability in the compact tension test, Int. J. Fract. Mech. **6**(1970), 189-192.

[13] Sherry, A.H., France, C.C., Goldthorpe, M.R., Compendium of T-stress solutions for two and three- dimensional cracked geometries, Engng. Fract. Mech. **18**(1995), 141-155.

[14] Newman, J.C., Stress analysis of compact specimens including the effects of pin loading, ASTM STP 560, 1974, 105.

[15] Srawley, J.E., Wide range stress intensity factor expressions for ASTM E399 standard fracture toughness specimens, Int. J. Fract. Mech. **12**(1976), 475-476.

[16] Noda, N.A., Oda, K., Numerical solutions of the singular integral equations in the crack analysis using the body force method, Int. J. Fract. **58**(1992), 285-304.

[17] Isida, M., Nishino, T., Formulae of stress intensity factor of bent cracks in plane problems, Trans. Japan. Soc. Mech. Engrs. 48/430(1982), 729-738.